METAL COMPLEXATION BY PHYTOCHELATINS AND MICROCYSTINS: A MOLECULAR DYNAMICS INVESTIGATION

A Thesis

Presented to the Faculty of the Graduate School

of Cornell University

In Partial Fulfillment of the Requirements for the Degree of

Master of Science

in

Environmental Toxicology

by

Amy Louise Pochodylo

May 2014

ABSTRACT

A better understanding of the metal–peptide complexes formed by phytochelatins and microcystins is necessary to understand the role of these peptides in algal cells and cyanobacteria, respectively. As there are limited structural and thermodynamic data on these metal–peptide complexes, molecular simulations may provide useful insights by providing structural insights in concert with thermodynamic stability predictions. I conducted molecular dynamics simulations of complexes of phytochelatin (n=2), microcystin-LR, and microcystin-RR with Ca^{2+}, Mg^{2+}, Fe^{2+}, Zn^{2+}, and Cu^{2+}. Structural characteristics of the resulting complexes agreed with results from other metal–peptide complexes. The simulation results also indicate that all three peptides bind Cu and Zn preferentially, supporting the peptides' roles in metal regulation. Peptide conformational changes after metal complexation shed light on the hypothesized transporters of the complexes from the cell, as well as on the environmental chemodynamics of the complexes and peptides in surface waters.

BIOGRAPHICAL SKETCH

Amy Louise Pochodylo earned her Bachelor of Science degree in Chemistry with Honors with an Environmental Studies Specialization from Lyman Briggs College at Michigan State University in 2013. She was named a 2011 Goldwater Scholar and a 2013 Alpha Chi Sigma Scholar. She has previously published fourteen articles in the field of inorganic chemistry in journals including *CrystEngComm* and *Crystal Growth & Design*. Her thesis research was supervised by Dr. Ludmilla Aristilde.

To Jake, for being my partner in all things. To my parents, for supporting me every step of the way. To Dr. LaDuca, for inspiring me to pursue science and research.

ACKNOWLEDGMENTS

I would like to express my gratitude to my advisor Dr. Ludmilla Aristilde for supporting me throughout this research project. I would also like to thank Dr. Beth Ahner for insightful comments and for serving on my committee. Lastly, I am grateful to David Flannelly and Thalia Aoki for technical assistance.

TABLE OF CONTENTS

LIST OF FIGURES

Chapter 1

Chapter 2

Chapter 3

Appendix A

Appendix B

Appendix C

LIST OF TABLES

Chapter 2

Chapter 3

LIST OF ABBREVIATIONS

CN	Coordination number
COMPASS	Condensed-phase Optimized Molecular Potentials for Atomistic Simulation Studies
EDTA	Ethylenediaminetetraacetic Acid
EM	Energy Minimization
MC	Microcystin
MC-LR	Microcystin-LR
MC-RR	Microcystin-RR
MD	Molecular dynamics
PC	Phytochelatin
PC-2	Phytochelatin (n=2)
RDF	Radial distribution Function

CHAPTER 1

INTRODUCTION

In all organisms, metal cations mediate important functions because of their role as cofactors for many enzymes.[1] In photosynthetic organisms, specifically, a variety of metal cations are essential for the proper function of the photosynthetic electron transport chain. Hundreds of chlorophyll molecules, which are essential for light absorption and energy transfer in the chloroplast, contain a Mg ion at their core.[2] Plastocyanin, a Cu–containing protein, shuttles electrons between cytochromes and photosystem I in the photosynthetic pathway.[3,4] The electron transport systems in both mitochondria and chloroplasts rely on ferredoxins, which contain Fe–S in their catalytic centers, and thus require ample supplies of Fe.[5] Superoxide dismutase, an essential enzyme which prevents the accumulation of superoxides generated during photosynthesis, requires both Cu and Zn for catalysis.[6] Zinc also participates in the regulation of gene expression.[7] Despite the important roles of trace metals in physiological functions, excess amounts can be cytotoxic by disrupting the redox balance in the cell and interfering with enzyme function. For instance, high levels of Cu and Fe can induce oxidative stress in plants.[5] Excess Zn can displace Fe, Mn, and Cu, causing metal deficiencies in plants.[5] High levels of Cd and Cu can interfere with phosphorus uptake, limiting plant growth.[8]

Higher plants, algae, and cyanobacteria produce peptides and organic ligands to regulate toxic metal levels via chelation.[9] Of particular interest are phytochelatins (PCs), which are produced by plants and algae in response to high levels of metals such as Cd, Cu, Pb and Zn.[10] These molecules are oligomers of ɣ–glutamyl-cysteine,

which are synthesized from glutathione, and generally have 2-11 repeated units (namely, PC-2 to PC-11).[11] In algae, PCs tend to be shorter with 2-4 repeat units (Figure 1A).[10] During times of metal stress, PCs bind the metal of concern and thus lower the level of metal toxicity in both the intracellular and extracellular milieu.[10,12] The efficiency of PCs in metal detoxification is due to the presence of multidentate binding sites via carboxylates and, at basic pH, the dissociated sulfhydryl groups.[13] Cyanobacteria are reported to synthesize and release small peptides including microcystins (MCs).[14] There are over 80 variants of MCs arising from two variable amino acids within the heptapeptide chain of MCs.[14] Two common MCs are MC-LR and MC-RR (Figures 1B and 1C), which contain, respectively, a lysine and an arginine or two arginine residues. The physiological role of MCs remains unclear, but there are two major hypotheses. One suggests that MCs are allelopathic compounds because they have been shown to be toxic to several organisms that consume cyanobacteria.[15] A second hypothesis proposes a role for MCs as metal regulators, similar to PCs, given their multiple carboxylate moieties. In accordance with this hypothesis, MCs have been shown to form complexes with a variety of metal ions, including Mg, Fe(II), Fe(III), Zn(II), and Cu(II).[16–18] Although a putative MC transporter gene (*mcyH*) is present in the MC gene cluster, MCs are primarily released upon cell lysis.[19,20] Interestingly, intracellular MCs populate the area around polyphosphate bodies in the cell, which are sites that require metal detoxification.[21] Thus, it is possible that MCs help regulate metal levels around these bodies.

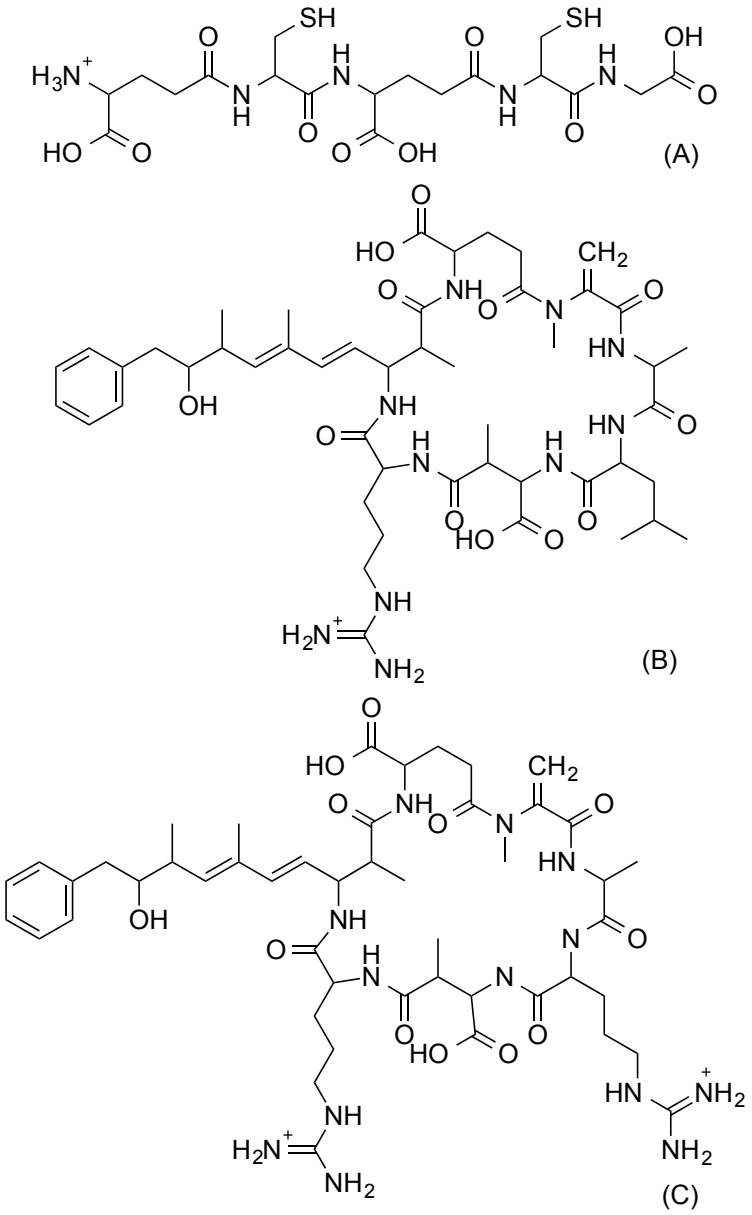

Figure 1. Chemical structure of phytochelatin-2 (A), microcystin-LR (B), and microcystin-RR (C).

In sum, there is clear evidence that both PCs and MCs can be involved in metal complexation. An in-depth structural examination of the hydrated structures of metal complexes with PCs and MCs is still warranted in order to gain insights into the physiological role of these peptides. However, the structures of these metal–peptides have not been fully characterized. Previous studies have focused on determining

thermodynamic parameters, such as stability constants of metal binding by PCs[13,22] and MCs.[16–18,23] X-ray absorption studies[11,22] of Cd–PC complexes have examined the Cd binding coordination but these studies have not provided structural information on the entire complex. Furthermore, structural studies of PC complexes with other metals are lacking. While there are several putative transporters for PCs[24,25] and there is an apparent transporter gene in the MC gene cluster,[19] there are currently, to the best of my knowledge, no structural confirmations of these transporters. Knowledge of the overall conformational dynamics of each peptide with and without the complexed metal can inform on the characteristics of the hypothesized transporters involved in transporting PC and MC. Moreover, thermodynamic data in concert with structural data will aid in further determining the intracellular role of MCs, a requisite to proper management of cyanobacterial blooms in an effort to reduce the production and environmental impact of the hepatotoxic MCs. Elucidating the structures of aqueous metal–PC and metal–MC complexes can also provide insight into the fate of these peptides in surface waters, where they can chelate metal ions and interact with particles in surface waters and sediments.[26–28]

Given the limited structural determinations of metal–PC and metal–MC complexes, molecular simulations can be useful in linking thermodynamic parameters with structural characteristics of these complexes. Here I combined Monte Carlo, energy minimization, and molecular dynamics algorithms to obtain energy– and geometry–optimized structures of aqueous complexes of PC-2, MC-LR, and MC-RR with five divalent metal cations: Ca, Mg, Fe(II), Zn(II), and Cu(II). The objectives of this study were to determine the relative binding affinities of the different peptides for

the different metals, characterize the structures of the metal coordination, and probe conformational changes in the peptide as a result of metal chelation. The simulation results provide structural insights towards a comprehensive understanding of the biological and environmental fate of PCs and MCs within the context of metal complexation.

CHAPTER 2

COMPUTATIONAL METHODS AND VALIDATION

Modeling Platform

Simulations were conducted using the all-atom Condensed-phase Optimized Molecular Potentials for Atomistic Simulation Studies (COMPASS; Accelrys, San Diego, CA, USA)[29] force field as implemented in the Forcite module of the Materials Studio software package.[30] This force field previously demonstrated[29,31,32] accurate simulations of structural properties of both simple and complex organic compounds, as well as metal complexation.[33] I also performed validation studies with the molecules simulated in the present study: phytochelatin (PC), microcystin (MC), and divalent metal cations [Ca, Mg, Fe(II), Zn(II), Cu(II)].

Validation Studies

To validate the use of the COMPASS force field in the present study, PC-2 and MC-LR were subjected to a series of simulations consisting of geometry optimization, energy minimization (EM), and annealing molecular dynamics (MD) in an effort to reach the global energy minimum. Thermodynamic and structural data were retrieved from a final MD, which was carried out in a canonical NVT ensemble (fixed number of atoms, simulation cell volume, and constant temperature) for 500 ps (time step = 1 fs) using a canonical thermostat algorithm to control temperature at 298 K. For all systems, the potential energy profile indicated that equilibrium was reached after 50 ps. Because there were no structural data for PC, which is an oligomer of glutathione,[34] the structure of the optimized PC was compared to that of glutathione[35] (Table 1). The experimental bond lengths in Table 1 correspond to the similar bond

lengths in glutathione, which is only one glutamine and one cysteine. Thus, the experimental lengths repeat for the two repeat units. Of the 34 bonds monitored for validation of PC-2, 26 were within one standard deviation of the literature value, and 7 others were within two standard deviations. Thus, the PC-2 structure was deemed valid in the COMPASS forcefield. Optimized structures of MC-LR were compared to available published structures of MC-LR[36] (Table 2). Of the 24 bonds in the MC-LR monitored for validation, all were within one standard deviation of the literature value. Because no structural data were available for MC-RR, the accurate simulation of MC-LR was considered evidence that COMPASS was a valid force field to simulate MC–RR. For solvated complexes of the metal cations, a previous study[33] demonstrated that COMPASS was adequate for simulating hydration of Ca, Mg, and Fe(II). In addition to repeating these prior simulations, we performed simulations of water complexes with Zn(II) and Cu(II). First, 150 water molecules were placed around the metal cations using the Adsorption Locator module. The resulting hydrated system was then subjected to a MD step for 1 ns (time step = 1 fs), using the same canonical ensemble described previously. Based on comparisons to published structural data for solvated metal ion complexes[37,38] (Table 3), COMPASS was proven to be a valid force field for all the metal cations solvation complexes investigated in the present study.

Table 1. Bond lengths (Å, average ± STD) in the PC-2 molecule.

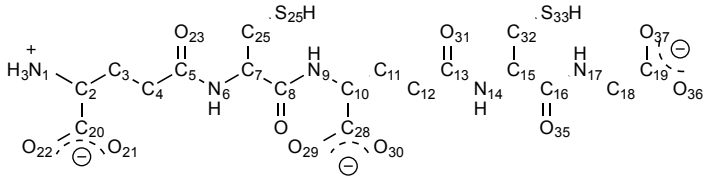

	Experiment[35]	*MD simulation*		*Experiment*[35]	*MD simulation*
C_{20}–O_{21}	1.243	1.238 ± 0.022	C_{28}–O_{29}	1.259	1.238 ± 0.019
C_{20}–O_{22}	1.264	1.240 ± 0.022	C_{28}–O_{30}	1.254	1.240 ± 0.022
C_{20}–C_2	1.524	1.557 ± 0.034	C_{10}–C_{11}	1.523	1.554 ± 0.037
C_2–N_1	1.445	1.517 ± 0.035	C_{11}–C_{12}	1.518	1.553 ± 0.031
C_2–C_3	1.523	1.541 ± 0.034	C_{12}–C_{13}	1.513	1.554 ± 0.031
C_3–C_4	1.518	1.551 ± 0.034	C_{13}–O_{31}	1.194	1.220 ± 0.018
C_4–C_5	1.513	1.552 ± 0.033	C_{13}–N_{14}	1.361	1.359 ± 0.029
C_5–O_{23}	1.194	1.221 ± 0.018	N_{14}–C_{15}	1.471	1.488 ± 0.035
C_5–N_6	1.361	1.342 ± 0.025	C_{15}–C_{32}	1.517	1.538 ± 0.029
N_6–C_7	1.471	1.483 ± 0.034	C_{32}–S_{33}	1.824	1.831 ± 0.039
C_7–C_{24}	1.517	1.531 ± 0.030	C_{15}–C_{16}	1.521	1.577 ± 0.035
C_{24}–S_{25}	1.824	1.829 ± 0.040	C_{16}–O_{35}	1.229	1.222 ± 0.019
C_7–C_8	1.521	1.500 ± 0.035	C_{16}–N_{17}	1.351	1.362 ± 0.027
C_8–O_{27}	1.229	1.222 ± 0.022	N_{17}–C_{18}	1.474	1.487 ± 0.033
C_8–N_9	1.351	1.397 ± 0.030	C_{18}–C_{19}	1.515	1.565 ± 0.031
N_9–C_{10}	1.474	1.470 ± 0.034	C_{19}–O_{36}	1.259	1.238 ± 0.020
C_{10}–C_{28}	1.515	1.601 ± 0.039	C_{19}–O_{37}	1.254	1.234 ± 0.020

[35] (Kassaar et al., 2014)

Table 2. Bond lengths (Å, average ± STD) in the MC-LR molecule.

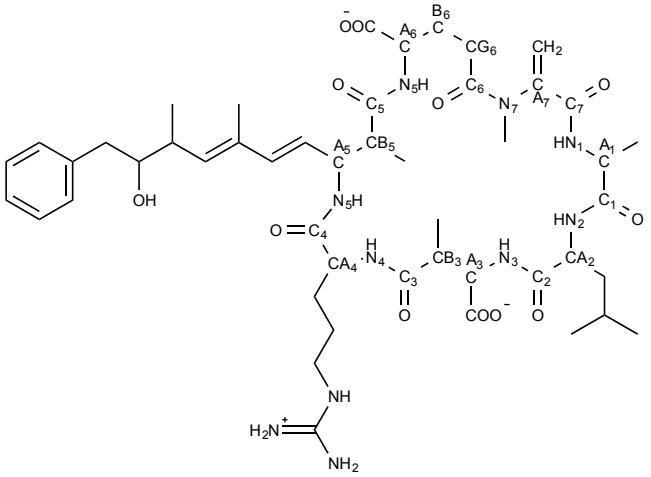

	Experiment [36]	*MD simulation*		*Experiment* [36]	*MD simulation*
N_1–CA_1	1.49	1.47 ± 0.03	N_5–CA_5	1.491	1.47 ± 0.03
CA_1–C_1	1.552	1.56 ± 0.03	CA_5–CB_5	1.577	1.56 ± 0.04
C_1–N_2	1.348	1.36 ± 0.03	CB_5–C_5	1.559	1.53 ± 0.04
N_2–CA_2	1.49	1.48 ± 0.04	C_5–N_6	1.347	1.35 ± 0.03
CA_2–C_2	1.551	1.50 ± 0.03	N_6–CA_6	1.490	1.47 ± 0.03
C_2–N_3	1.348	1.36 ± 0.04	CA_6–CB_6	1.563	1.54 ± 0.03
N_3–CA_3	1.489	1.48 ± 0.03	CB_6–CG_6	1.549	1.54 ± 0.03
CA_3–CB_3	1.573	1.56 ± 0.04	CG_6–C_6	1.550	1.55 ± 0.03
CB_3–C_3	1.556	1.53 ± 0.03	C_6–N_7	1.372	1.38 ± 0.04
C_3–N_4	1.348	1.36 ± 0.03	N_7–CA_7	1.470	1.48 ± 0.03
N_4–CA_4	1.490	1.47 ± 0.03	CA_7–C_7	1.551	1.54 ± 0.03
CA_4–C_4	1.551	1.57 ± 0.03	C_7–N_1	1.348	1.38 ± 0.03

[36] (Bagu et al., 1995)

Table 3. Metal cation–OH_2 distances (Å, average ± STD) in solvation complexes.

	Experiment	*MD simulation*
Ca^{2+}–OH_2	2.41–2.46[37]	2.40 ± 0.09
Mg^{2+}–OH_2	2.05–2.15[37]	2.00 ± 0.06
Fe^{2+}–OH_2	2.12–2.28[38]	2.02 ± 0.08
Zn^{2+}–OH_2	2.08–2.15[38]	2.03 ± 0.08
Cu^{2+}–OH_2	1.96–2.10[38]	2.00 ± 0.05

[37] (Vinogradov et al., 2003) [38] (Ohtaki and Radnai, 1993)

Simulations of metal-PC and metal-MC complexes

We performed simulations of MC and PC with Ca, Mg, Fe(II), Cu(II), or Zn(II) in a hydrated environment. For metal–PC complexes, one metal ion was used with PC-2, which has an overall charge of –2 arising from three deprotonated carboxylic acid groups and one protonated amino group. Deprotonated sulfhydryl groups were not considered here because the COMPASS forcefield lacks a description for a negatively charged sulfide. The model with protonated sulfhydryl groups would still be relevant because intracellular pH in algae and cyanobacteria is reported to be between 6.2–8,[39–41] and two other studies reported the pK_a of the cysteine thiol group in the PC-2 to be greater than 8.59.[13,42] Thus, it is reasonable to expect that not all the sulfhydryl groups would be fully deprotonated over the entire intracellular pH range. In fact, an X-ray absorption examination of Cd–PC complexes[11] revealed that binding coordination was only from PC O atoms at acidic pH and, at basic pH, from a combination of S and O atoms from PC, especially when the ratio of Cd to PC is high. For the simulations of metal–MC complexes, the protonated guanidinium groups of the arginine residues were charge balanced with Cl^-, while the carboxylate groups were balanced with the metal cations.

The modeling workflow executed for each metal–peptide complex is illustrated in Figures 2A and 2B.

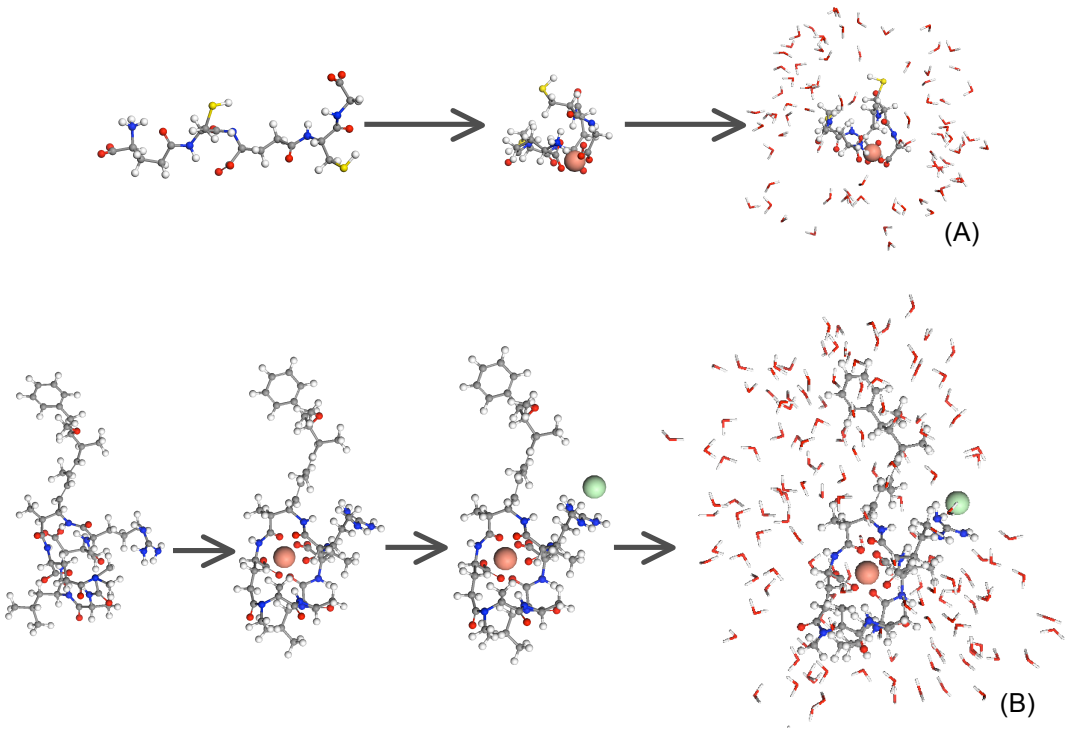

Figure 2. Modeling workflow for obtaining preliminary structures of metal complexes with PC-2 (A) and MC-LR (B). In A, from left to right: optimized PC-2, Cu–PC-2 complex after adsorption and first MD run, and hydrated system after last MD run. In B, from left to right: optimized MC-LR, Cu–MC-LR after adsorption and first MD run, Cu–MC-LR with Cl^- placed by guanidinium group, and hydrated system after last MD run. Same procedure described in B was used for MC-RR.

For each case, the metal cation was first adsorbed to the peptide molecule using the Adsorption Locator module in Materials Studio. This module subjected the metal cation to both translation and rotation steps via an annealing Monte Carlo search[30] with a temperature cycle from 300 K to 800 K, repeated ten times. After metal adsorption onto the peptide molecule, the system was subjected to MD equilibration for 1 ns (time step = 1 fs) at 298 K using the same canonical ensemble described above. Following this step for the systems with MC, the chloride ions were placed near the guanidinium groups of the arginine residues based on experimentally determined interaction distances.[43] Subsequently, a hydrated environment of each fully

charge–compensated metal–peptide complex was achieved by creating a shell of explicit water molecules in a nonperiodic system. Each hydrated system was subjected to a final MD simulation for 1 ns (time step = 1 fs), from which thermodynamic and structural data were retrieved. Potential energy profiles indicated equilibrium occurred after 400 ps for the metal–PC complex and after 100 ps for the metal–MC complex.

The COMPASS force field calculates total potential energies that include both non-bond and valence contributions. Because the energy parameters in COMPASS are not referenced to a unique molecular state, these calculated energies can be compared relatively within a given set of simulations but not to experimentally determined potential energies.[44] Total potential energies for the metal–peptide complexes, excluding the contributions of the water-water interactions, were used to evaluate the relative thermodynamic stability of each molecule to complex the different metals.[33] All configurations obtained for the solvated metal–peptide complexes after equilibration of the total potential energy were used to compute statistics for the calculated energies and the interatomic distances between O atoms and the metal cations. To understand the local environment of metal complexation in each metal–peptide complex, radial distribution functions (RDFs) for metal cation–O atom pairs were obtained using the lowest–energy equilibrated configuration. To determine the coordination numbers (CNs), the RDFs for metal cation–carboxylate O, metal cation–carbonyl O, and metal cation–water O were determined by integrating the RDFs from the origin out to the first minimum with a bin interval of 0.02 Å.[44] Using the Discovery Studio software package,[45] surface potential maps of PCs and

MCs were obtained, following removal of all hydrating waters and metal and chloride ion, by employing a marching cubes algorithm to create an isopotential surface based on the localization of atom charges in the peptide conformation. The surface potential map was created based on the lowest-energy equilibrated configuration obtained during the final MD step.

CHAPTER 3

RESULTS AND DISCUSSION

Metal complexation by PC-2

The total potential energy calculated for Ca–PC-2, Mg–PC-2, Fe–PC-2, Zn–PC-2, and Cu–PC-2 was –415 ± 9, –452 ± 8, –515 ± 6, –519 ± 9, and –523 ± 9 kcal/mol, respectively. Thus, the relative ordering of stability for the simulated metal–PC-2 complexes was Cu–PC-2 ≥ Zn–PC-2 ≥ Fe–PC-2 > Mg–PC-2 > Ca–PC-2. Because of limited experimental data on stability constants for metal–PC complexes, I compared the simulated series with previous studies on metal complexes with glutathione[46,47] and ethylenediaminetetraacetic acid (EDTA).[48] Similar stability constants were reported for complexes of glutathione, a building block of PC, with Cu(II) and Zn(II).[46,47] EDTA, a strong metal chelator with multiple carboxylate binding sites, exhibits the most stable complex with Cu(II) followed by, in order of decreasing stability constants, Zn(II), Fe(II), Ca, and Mg.[48] These trends in stability constants are congruent with the energy data retrieved from the MD–optimized metal–PC complexes. It was reported that PCs are released when algae are under stress from toxic levels of trace metals such as Cd, Cu, Pb, and Zn.[10] The fact that the PC-2 complexes with Cu(II), Zn(II), and Fe(II) were the most stable is in accordance with the role of PC-2 as an efficient chelator of these trace metals. The thermodynamic data from the simulations also indicated that PCs are not likely used to regulate alkali earth metals such as Ca and Mg, which do not induce metal stress at the same levels as trace metals.[49] As previously reported in an MD study of metal complexation by an antibiotic carboxylate,[33] the total potential energies of the metal–PC-2 complexes

generally varied inversely with metal cationic ionic potentials, a trend that is consistent with the role of electrostatic interactions in mediating stability of the complex.

The binding coordination of the metal in each metal–PC-2 complex was characterized in an effort to account for the structures responsible for the estimated thermodynamic stability. Specifically, I obtained the RDFs of the O atoms from carboxyl, carbonyl, and solvating waters around each metal cation (Figure 3). The RDFs of metal–PC-2 carboxylate O indicated that carboxylate O atoms were at greater than 2.00 Å from Ca^{2+} whereas they were between 1.70 and 2.00 Å from Mg^{2+}, Fe^{2+}, Zn^{2+}, and Cu^{2+} (Figure 3, Table 4). For the RDFs of metal–PC-2 carbonyl O, only Ca^{2+}, Mg^{2+}, and Zn^{2+} had carbonyl O atoms at short enough interaction distances to be involved in complexation, which were, on average, 2.47, 2.21, and 2.00 Å, respectively. The carbonyl O atoms were greater than 3.00 Å away from the other metal cations (Figure 3, Table 4). The distance of the carboxylate O atoms from the metal cations was positively correlated with the ordering of stability predicted by the MD–calculated thermodynamics of the complexes, in agreement with the proposed role of electrostatic interactions. In terms of the role of hydrating waters, the RDFs indicated water O atoms at less than 2.5 Å only near Mg^{2+}; the remainder of the RDF peaks for water O atoms at greater than 3.0 Å from the metal cations were reminiscent of the water structures in bulk water[50] (Figure 3, Table 4). Based on the integration of the RDFs, the number of O atoms around each metal ion was determined (Table 4). The MD simulation predicted a Ca–PC-2 complex wherein Ca^{2+} coordinated to a total of six O atoms: four from carboxylate moieties and two from keto (carbonyl) groups

(Table 4, Figure 4). The Mg–PC-2 complex had Mg^{2+} coordinated to five total O atoms, with three carboxyl O atoms and one each from a carbonyl and solvating water. The Fe^{2+} in the Fe–PC-2 complex was coordinated to six total O atoms, all from carboxylate moieties (Table 4, Figure 4). In the Zn–PC-2 complex, the Zn^{2+} was coordinated to five O atoms, with four coming from carboxylate moieties and one from a keto group (Table 4, Figure 4). In the Cu–PC-2 complex, Cu^{2+} coordinated to a total of five O atoms, all from carboxylate moieties (Table 4, Figure 4).

Table 4. Distance (Å, average ± standard deviation) and coordination numbers (CNs) calculated for metal cation-O atom pairs in metal-PC-2 complexes by molecular dynamics simulations.

Metal—PC-2						
Metals	Metal—$O_{carboxylate}$		Metal—$O_{carbonyl}$		Metal—O_{water}	
	Distance	CN	Distance	CN	Distance	CN
Ca^{2+}	2.19 ± 0.15	3.99	2.47 ± 0.05	1.97	--	--
Mg^{2+}	1.76 ± 0.08	3.14	2.21 ± 0.12	0.86	2.23 ± 0.11	1.0
Fe^{2+}	2.02 ± 0.30	5.98	--	--	--	--
Zn^{2+}	1.79 ± 0.08	4.0	2.00 ± 0.05	1.0	--	--
Cu^{2+}	1.85 ± 0.14	4.88	--	--	--	--

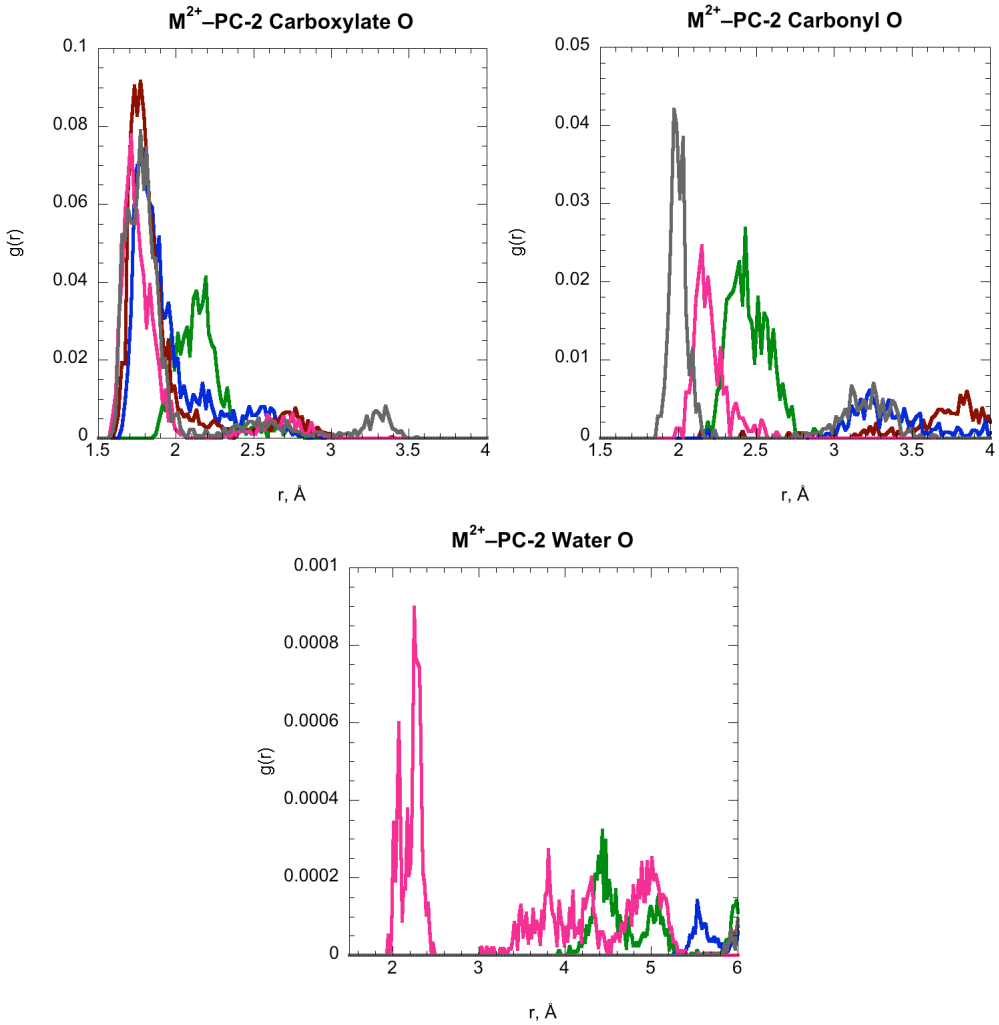

Figure 3. Metal cation-O radial distribution functions [RDFs, g(r)] for carboxylate O, carbonyl O, and water O in the hydrated M^{2+}–PC-2 complexes. Line color legend: green (Ca^{2+}), pink (Mg^{2+}), blue (Fe^{2+}), brown (Cu^{2+}), gray (Zn^{2+}).

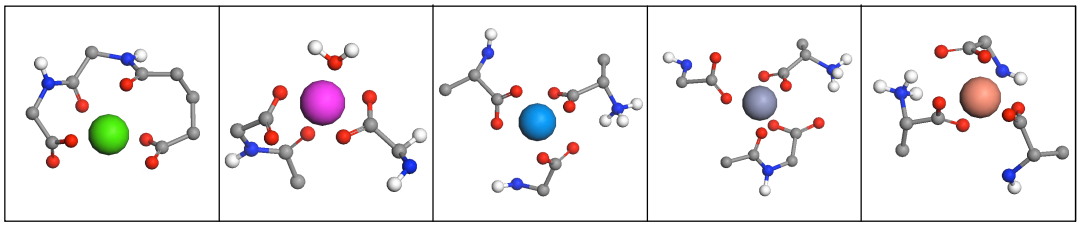

Figure 4. Molecular dynamics snapshots of metal coordination with O atoms from PC-2 and solvating water molecules. Non-coordinating water molecules and some atoms from the peptide structure were removed for clarity. Atom color legend: gray (C), red (O), white (H), green (Ca^{2+}), pink (Mg^{2+}), blue (Fe^{2+}), brown (Cu^{2+}), gray (Zn^{2+}).

To the best of my knowledge, there are no detailed experimental structural data available for metal–PC complexes with which to compare the simulation results. However, an X-ray absorption study[11] of Cd–PC complexes reported that, at acidic pH, all of the interactions between the metal cation and the PC were mediated by PC O atoms at a distance of about 2 Å. This Cd–PC O distance agrees with the M^{2+}–PC O distances predicted by my simulations. The suggested coordination of six O atoms around the Cd^{2+} ion[11] is also consistent with the coordination environments in the MD-optimized Ca– and Fe(II)–PC-2 complexes, both of which have metal ions with ionic potentials close to that of Cd^{2+}. It is important to note that, as the aqueous pH becomes more basic, there would be decreasing contributions from the PC O atoms and increasing complexation by the deprotonated thiol groups.[11,22] An X-ray diffraction study of Cu(II) with L-aspartate[51] reported a distance of 1.95 Å, in good agreement with the distances found between the carboxylate O atoms and the Cu^{2+} in the simulated Cu(II)–PC-2 complex. A review study[52] of metal–ligand interactions in proteins reported distances between metal and O atoms in agreement with the MD–determined distances between the coordinating carboxylate O atoms and metal cation in the structures obtained for Ca–, Fe(II)–, and Cu(II)–PC-2 complexes. However, my MD simulations of the Mg– and Zn(II)–PC-2 complexes both presented metal–carboxylate O distances which were shorter than the reported values with proteins.[52] It is worth noting that the metal cations in my simulated systems were complexed by multiple types of O atoms, with the carboxylate interaction distance being the shortest (Table 4, Figure 3).

Metal complexation by MCs

For MC-LR, the total potential energy calculated for Ca–MC-LR, Mg–MC-LR, Fe–MC-LR, Zn–MC-LR, and Cu–MC-LR was –543 ± 9, –578 ± 10, –594 ± 10, –617 ± 7, and –598 ± 13 kcal/mol, respectively. Therefore, the relative ordering of stability for the simulated metal–MC-LR complexes was Zn–MC-LR > Cu–MC-LR ≥ Fe–MC-LR ≥ Mg–MC-LR > Ca–MC-LR. The ordering of the stability of the metal–MC-LR complexes followed the general trend predicted by my simulations of the metal–PC-2 complexes. For the MC-RR complexes, the calculated total potential energy for Ca–MC-RR, Mg–MC-RR, Fe–MC-RR, Zn–MC-RR, and Cu–MC-RR was –698 ± 9, –765 ± 6, –647 ± 7, –777 ± 9, and –767 ± 11 kcal/mol, respectively. Thus, the relative ordering of stability for the simulated metal–MC-RR complexes is Zn–MC-RR ≥ Cu–MC-RR ≥ Mg–MC-RR > Fe–MC-RR > Ca–MC-RR. A study[16] using differential pulse polarography to determine formation constants of MC-LR, MC-LW (arginine replaced by tryptophan), and MC-LF (arginine replaced by phenylalanine) complexes with Cu(II) and Zn(II) reported a trend consistent with my MD predictions. Another study[23] which used anodic stripping voltammetry to examine MC-LR complexes with Pb(II), Cd(II), Cu(II), Hg(II), and Zn(II) reported that Zn(II) had a higher binding constant than Cu(II) with MC-LR, in agreement with my MD findings with both MC-LR and MC-RR. As found with PCs, the most stable metal–MC complexes were those formed with Cu^{2+} and Zn^{2+}. This suggests that MCs could potentially be involved in regulating toxic levels of these trace metals. However, whereas PCs are known to be exuded from the cell to control metal levels, MCs are

likely intracellular regulators in cyanobacterial cells, as they are primarily released in large amounts after cell lysis.[20]

The binding coordination of the metal cation in each metal–MC complex was also characterized to further elaborate on the role of the binding structures on dictating the thermodynamic stability. The RDFs of the water O atoms and the MC carboxyl and carbonyl O atoms are illustrated in Figure 5. The RDFs of metal–MC carboxylate O atoms indicated that in both the Ca^{2+}–MC-LR and Ca^{2+}–MC-RR complexes the carboxylate O atoms were greater than 2.00 Å from the metal cation (Table 5, Figure 5). In the other metal–MC complexes, the interaction distances were between 1.70 and 1.95 Å (Table 5, Figure 5), a slightly shorter distance than reported with the PC carboxylate O atoms. For the RDFs of carbonyl O atoms, all of the metal–MC complexes had interaction distances between 1.90 and 2.65 Å, except for Mg–MC-RR, which did not have any carbonyl O atoms within 3.00 Å of the metal cation (Table 5, Figure 5). Hydrating waters only played a role in the Fe–MC-RR complex, which had water O atoms, on average, 2.56 Å from the metal cation (Table 5, Figure 5). The remainder of the complexes had water O atoms at a distance beyond 3.00 Å, where the water molecules behaved as bulk water.[50] As with the metal–PC complexes, published structural data of metal–MC complexes were scarce. The interaction distances between carboxylate O atoms and metal cations in the Ca–, Fe(II)–, and Cu(II)–MC-LR complexes were in agreement with those published for other metal–peptide complexes (Table 5).[52] However, for the Mg– and Zn–MC-LR complexes as well as all of the metal complexes with MC-RR, the distances were shorter than reported for

other metal–peptide complexes[52] but still within a reasonable range for metal–O interaction distances (Table 5).

Based on the RDFs, the number of coordinated O atoms around each metal cation in the metal–MC complexes was determined. In Ca–MC-LR, Ca^{2+} was coordinated to seven total O atoms, with four carboxylate O atoms and three keto O atoms whereas in Ca–MC-RR, Ca^{2+} was coordinated to six total O atoms, with four coming from carboxylate moieties and two from keto groups (Table 5, Figure 6). In the Mg–MC-LR complex, Mg^{2+} was coordinated to five total O atoms, with three coming from carboxylate moieties and two from keto groups; the Mg^{2+} atom in the Mg–MC-RR complex was coordinated to only three O atoms, all coming from carboxylate moieties (Table 5, Figure 6). In both the Ca and Mg complexes with MC-RR, the MC-RR carboxylate distance was shorter than in the corresponding distance in MC-LR complexes, indicating a stronger contribution from carboxylate groups in MC-RR. In the Zn–MC-LR complex, the Zn^{2+} was coordinated to a total of five O atoms: two from carboxylate moieties and three from keto groups (Table 5, Figure 6). The Zn–MC-RR complex had a six–coordinated Zn^{2+}, with four O atoms from carboxylate groups and two from keto groups (Table 5, Figure 6). In both of the Cu(II)–MC complexes, the Cu^{2+} ion was coordinated to six O atoms. In the Cu–MC-LR complex, three O atoms were from carboxylate moieties and three from keto O atoms whereas, in the Cu–MC-RR complex, four O atoms were from carboxylate moieties and the remaining two were from keto groups (Table 5, Figure 6). Notably, the Cu^{2+}–carboxylate O distance in the MC-RR complex had a shorter interaction distance than that same interaction in the MC-LR complex and more carboxylate O atoms were

involved in the MC-RR complex, indicating that the driving interaction in MC-RR was the bidentate carboxylate groups. The Fe complexes were the most dissimilar between the two MC complexes. In Fe–MC-LR, the Fe^{2+} was coordinated to two carboxyl O atoms, one from each pair of carboxylate O atoms, and three carbonyl O atoms. The Fe–MC-RR, the Fe^{2+} was coordinated to two carboxyl O atoms, both from the same carboxylate group, one carbonyl O atom, and two solvating waters (Table 5, Figure 6). The Fe–MC-RR complex was less stable in comparison to other MC-RR complexes than the Fe–MC-LR complex was in comparison to MC-LR complexes. This may be due to the decreased contribution to the metal chelation from the MC-RR molecule, which only had three O atoms coordinated to the Fe^{2+}, compared to MC-LR, where the Fe^{2+} was coordinated to five O atoms from the MC molecule. A study[16] with MC-LR and two other MC variants, MC-LW and MC-LF, wherein the arginine is replaced by tryptophan or a phenylalanine residue, respectively, reported the same trend of stability constants for the three variants, thus suggesting that the protonated arginine group was not involved in the complexation of the metals, consistent with the simulation results.

Table 5. Distance (Å, average ± standard deviation) and coordination numbers (CNs) calculated for metal cation-O atom pairs in metal-MC complexes by molecular dynamics simulations.

Metal—MC-LR						
Metals	Metal—$O_{carboxylate}$		Metal—$O_{carbonyl}$		Metal—O_{water}	
	Distance	CN	Distance	CN	Distance	CN
Ca^{2+}	2.25 ± 0.13	3.94	2.64 ± 0.47	2.80	--	--
Mg^{2+}	1.81 ± 0.11	2.85	1.94 ± 0.07	1.99	--	--
Fe^{2+}	1.76 ± 0.03	1.98	2.06 ± 0.08	2.99	--	--
Zn^{2+}	1.75 ± 0.01	2.00	2.10 ± 0.19	3.00	--	--
Cu^{2+}	1.91 ± 0.29	2.98	2.08 ± 0.13	3.00	--	--
Metal—MC-RR						
Metals	Metal—$O_{carboxylate}$		Metal—$O_{carbonyl}$		Metal—O_{water}	
	Distance	CN	Distance	CN	Distance	CN
Ca^{2+}	2.01 ± 0.02	4.00	2.54 ± 0.02	1.99	--	--
Mg^{2+}	1.70 ± 0.05	3.14	--	--	--	--
Fe^{2+}	1.79 ± 0.04	2.00	2.33 ± 0.21	0.97	2.56 ± 0.17	2.00
Zn^{2+}	1.75 ± 0.03	3.97	2.25 ± 0.08	1.97	--	--
Cu^{2+}	1.72 ± 0.04	4.00	2.34 ± 0.11	1.67	--	--

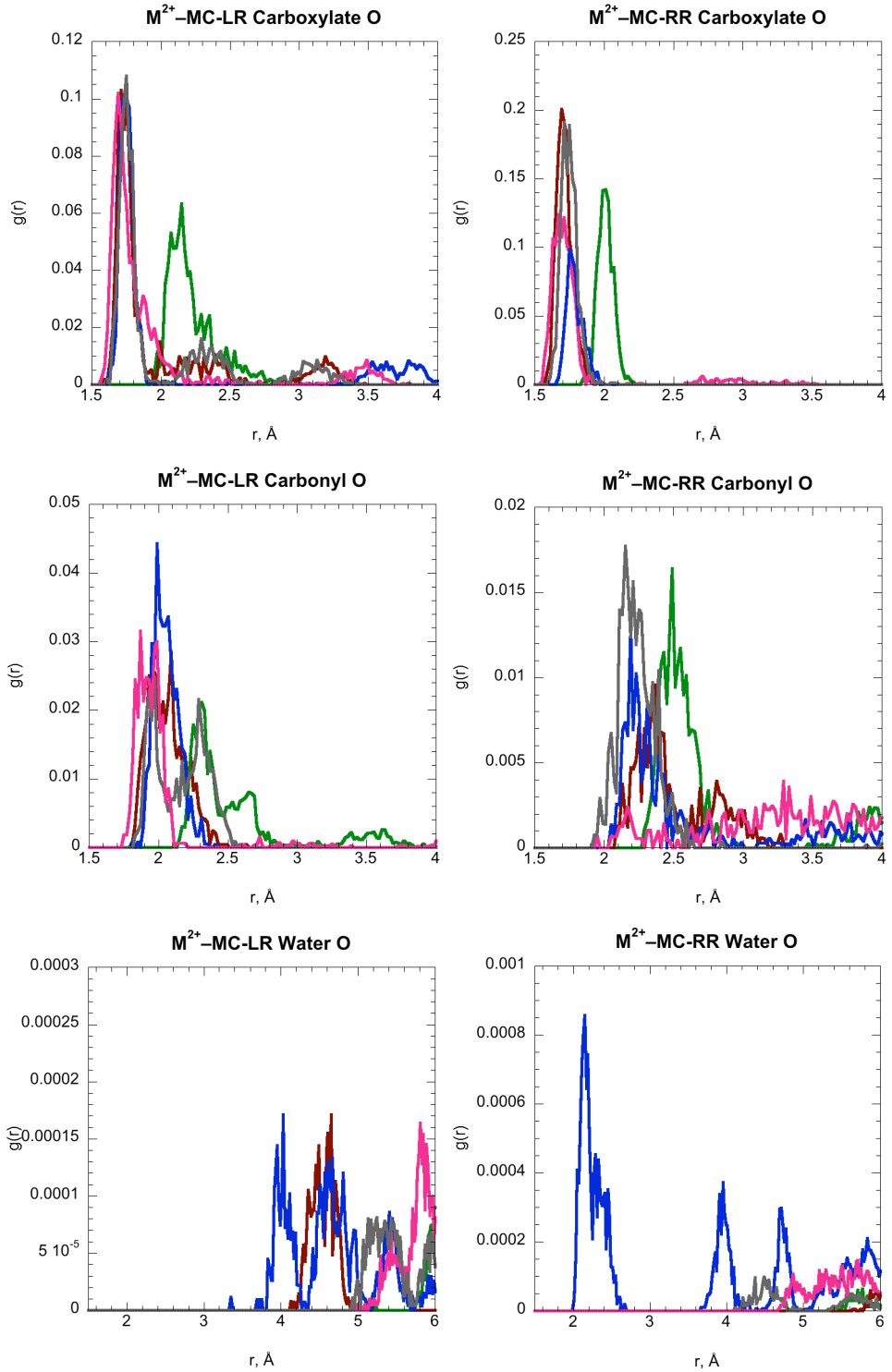

Figure 5. Metal cation-O radial distribution functions [RDFs, g(r)] for carboxylate O (top), carbonyl O (middle), and water O (bottom) in the hydrated M^{2+}–MC-LR and M^{2+}–MC-RR complexes. Line color legend: green (Ca^{2+}), pink (Mg^{2+}), blue (Fe^{2+}), brown (Cu^{2+}), gray (Zn^{2+}).

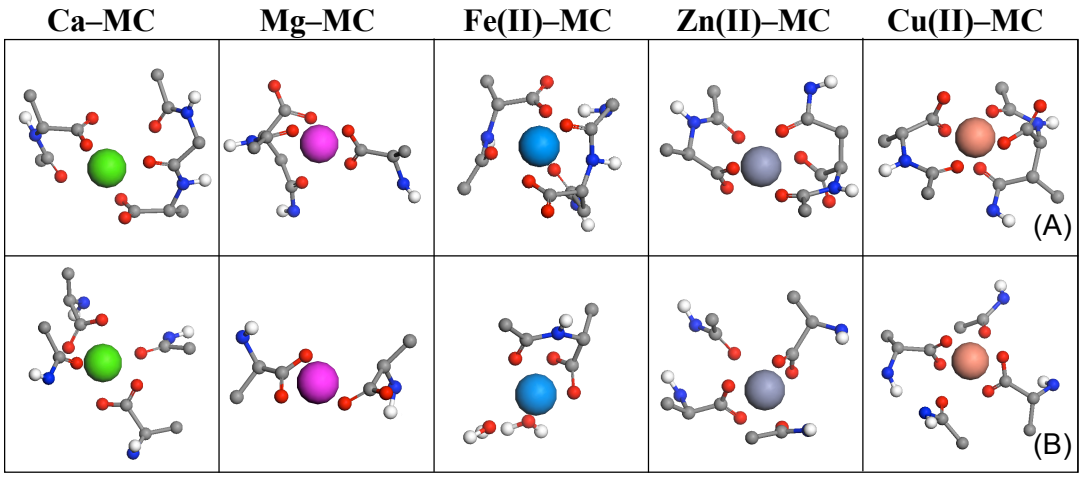

Figure 6. Molecular dynamics snapshots of metal coordination with the carboxylate and carbonyl moieties of MC and with solvating water molecules: MC-LR (A) and MC-RR (B). Non-coordinating water molecules and some atoms from the peptide structure were removed for clarity. Atom color legend: gray (C), red (O), white (H), green (Ca^{2+}), pink (Mg^{2+}), blue (Fe^{2+}), brown (Cu^{2+}), gray (Zn^{2+}).

Changes in Conformation

To investigate the distribution of hydrophobic and hydrophilic moieties across the different peptide molecules, surface potential maps before and after complexation with the different metal cations were computed (Figure 7). The PC-2 molecule had charged areas spread across it, indicating that the hydrophilic moieties were distributed across the surface of PC-2 (Figure 7). The broad distribution of charged areas across the PC-2 molecules indicated that the metal–PC-2 complexes formed intracellularly are not likely candidates for passive permeation across the cell membrane and that, in order for PC-2 to move into or out of the cell, a transporter would be necessary.[55] There were also variations in the potential maps of the metal–PC-2 complexes. All of the metal–PC-2 complexes, except for Mg–PC-2, have a

globular shape with a similar charge distribution, suggesting that the same transporter could be used for these peptide molecules (Figure 7).

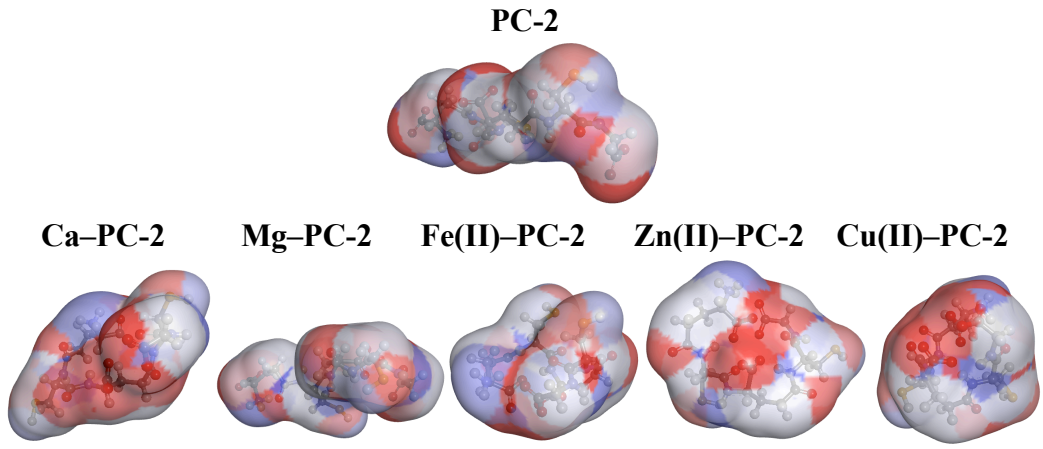

Figure 7. Surface potential maps of uncomplexed PC-2 (top) and the PC-2 structures in complexes with, from left to right, Ca, Mg, Fe(II), Cu (II), Zn (II). Red areas indicate negatively charged regions; blue areas are where positive charges are centered.

By contrast, the surface potential maps of the MC molecules were mostly characterized by neutral or hydrophobic areas (Figure 8). This mostly hydrophobic character of the MC molecules may be responsible for the lack of clear correlation, as discussed above, between SAV and the coordination distance with the carboxylate O atoms in the metal–MC molecules. Comparison of the surface potential maps of MC-LR (Figure 8) shows there was little variation amongst the different metal–MC-LR complexes, but more conformational changes were noticeable amongst the surface potential maps of the MC-RR complexes (Figure 8). The more linear structure of the MC-LR structures with positive charges generally clustered in the center suggests that it may be possible for these complexes to be transported via a transporter with a similar binding pocket for the MC-LR, especially given the similarity in the shape and

charge distribution of the uncomplexed MC-LR molecule (Figure 8). For the MC-RR complexes, the Cu(II) and Fe(II) complexes were different geometrically from the Ca, Mg, and Zn(II) complexes (Figure 8). In particular, the Fe(II)– and Cu(II)–MC-RR complexes exhibited a more globular conformation, which was distinct from the rest of the more linear metal–MC-RR complexes (Figure 8). These differences in geometries suggest that, if transporters were involved in exporting the MC-RR complexes, several would be required with different structural and chemical characteristics.

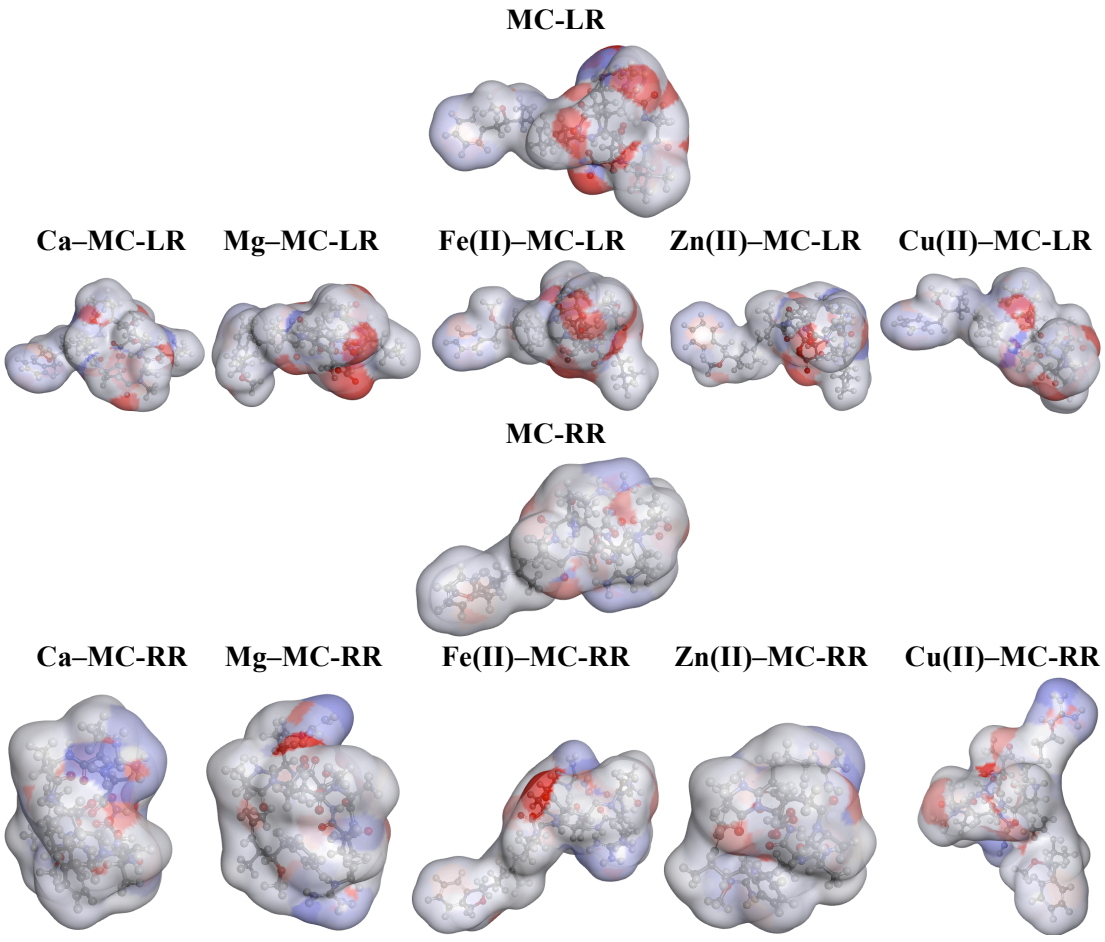

Figure 8. Surface potential maps of uncomplexed MC-LR and MC-RR and the MC-LR and MC-RR structures in complexes with Ca, Mg, Fe(II), Zn(II), and Cu(II). Positively charged areas are blue and negatively charged areas are red.

In this study, I characterized metal complexation and conformational dynamics in complexes of PC-2, MC-LR, and MC-RR with Ca, Mg, Fe(II), Zn(II), and Cu(II). The most stable complexes with all three peptides were formed with Zn^{2+} and Cu^{2+}, and the complexes with Ca^{2+} were the least stable. The similar stability order for both series of the MC complexes when compared with series of metal complexes with PC, which is known to chelate toxic metal ions, is congruent with the possible role of MCs in regulating toxic metal levels. In addition to informing on the characteristics of hypothesized transporters for the different peptides, the surface potential maps provide insights into possible mechanisms of interactions by the peptides with organic and inorganic particles in surface water. For instance, the positively charged areas in PC and MC may mediate interactions with the negatively-charged surfaces of minerals and organo-mineral particles in sediments.[56] On the other hand, the presence of hydrophobic moieties in MCs may facilitate partitioning of MCs and metal–MC complexes within hydrophobic regions of organic matter surrounding the cyanobacterial cells. Previous studies have determined that PCs are produced in response to toxic levels of metals,[10] and the binding sites of PC–Cd complexes have been characterized.[11,13] Other studies have also qualitatively examined metal–MC complexes,[17] and several have determined quantitative stability constants for Fe–, Zn(II)– and Cu(II)–MC complexes.[16,18,23] My MD simulation work provides the first detailed structural characterization of metal complexes with PCs and MCs using MD techniques. Future experimental studies on the complexation of various metal cations with both PC and MC variants are warranted in order to affirm the characteristics of the metal–peptide complexes presented here and to further elucidate the biological

roles of these peptides, as well as to better understand their environmental fate when exuded from their host cells.

APPENDIX A

STRUCTURES OF METAL–PC-2 COMPLEXES

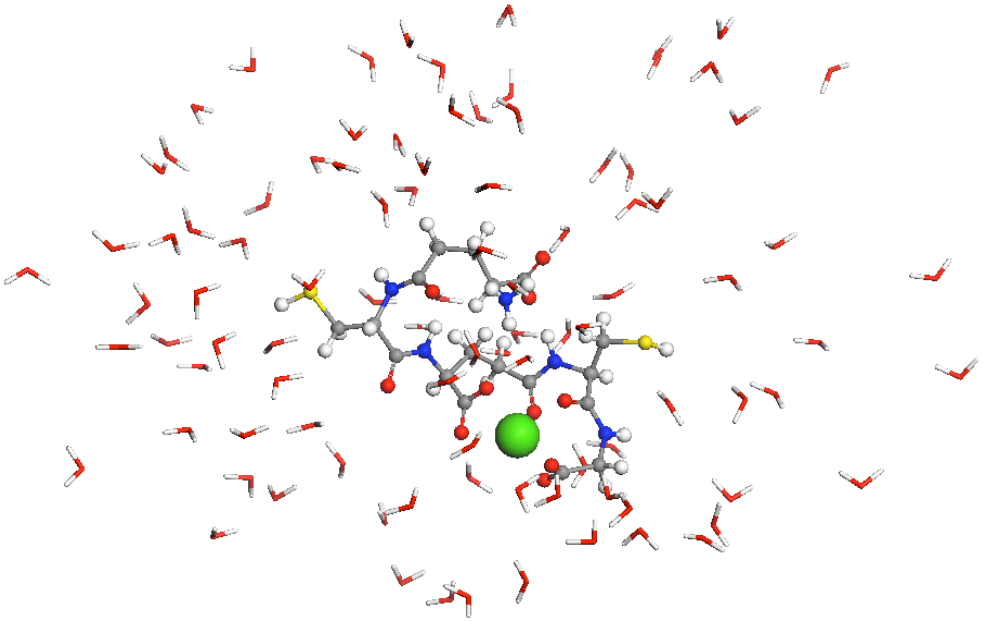

Figure S1. Fully hydrated Ca–PC-2 complex after last MD run. Atom color legend: gray (C), red (O), white (H), yellow (S), green (Ca^{2+}).

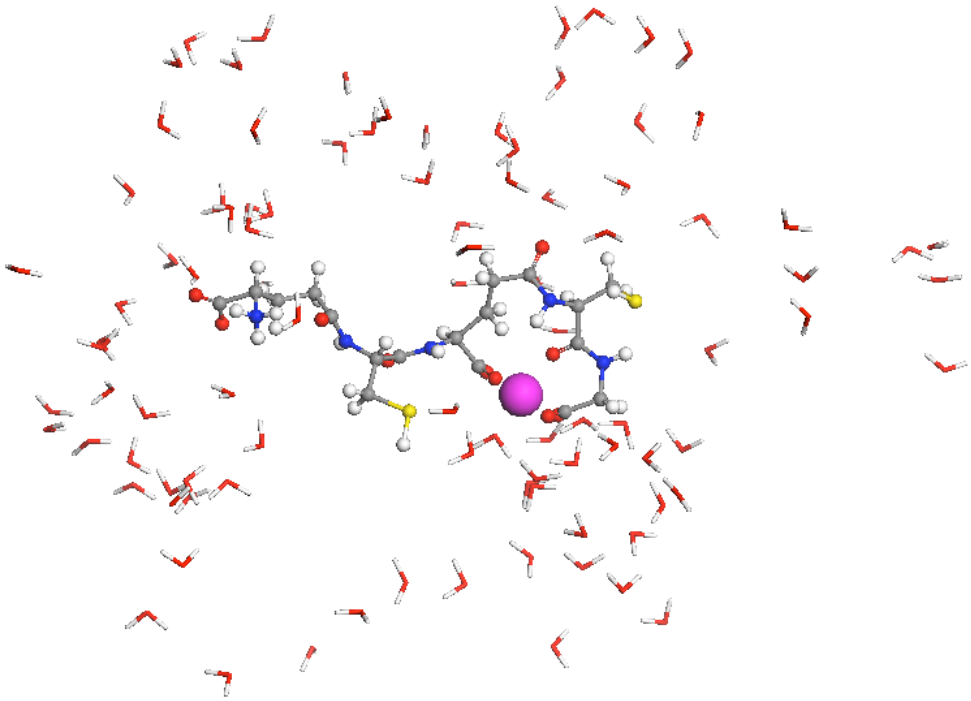

Figure S2. Fully hydrated Mg–PC-2 complex after last MD run. Atom color legend: gray (C), red (O), white (H), yellow (S), pink (Mg^{2+}).

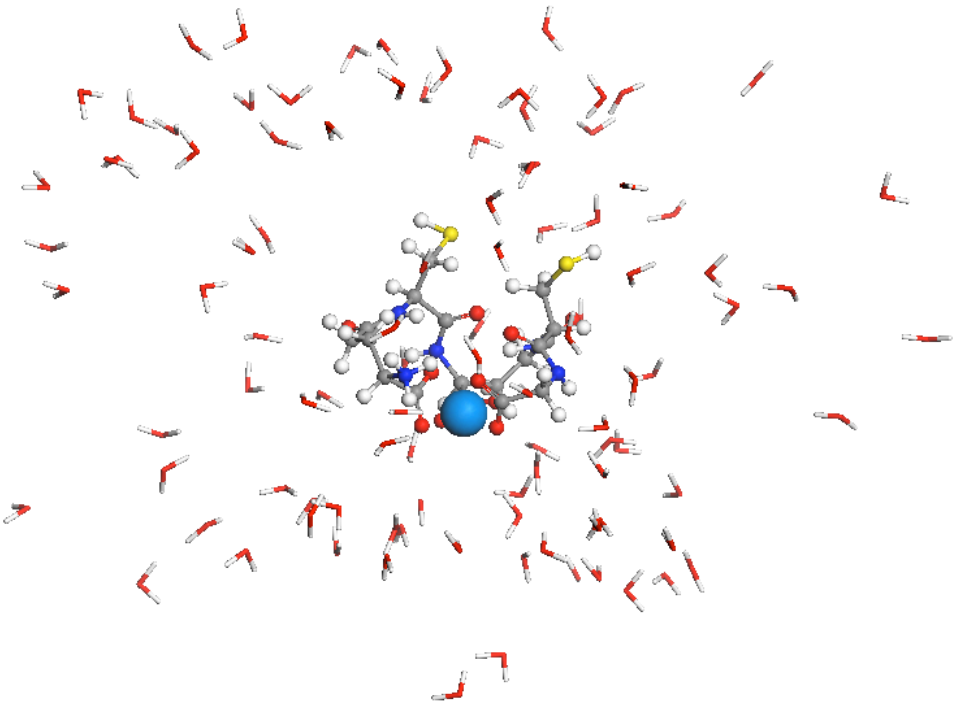

Figure S3. Fully hydrated Fe(II)–PC-2 complex after last MD run. Atom color legend: gray (C), red (O), white (H), yellow (S), blue (Fe^{2+}).

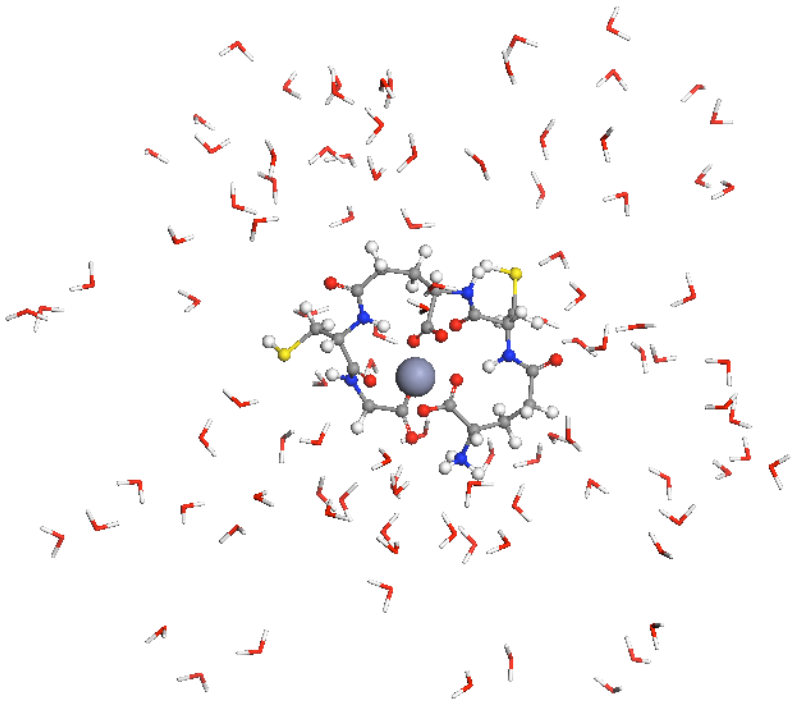

Figure S4. Fully hydrated Zn(II)–PC-2 complex after last MD run. Atom color legend: gray (C), red (O), white (H), yellow (S), gray (Zn^{2+}).

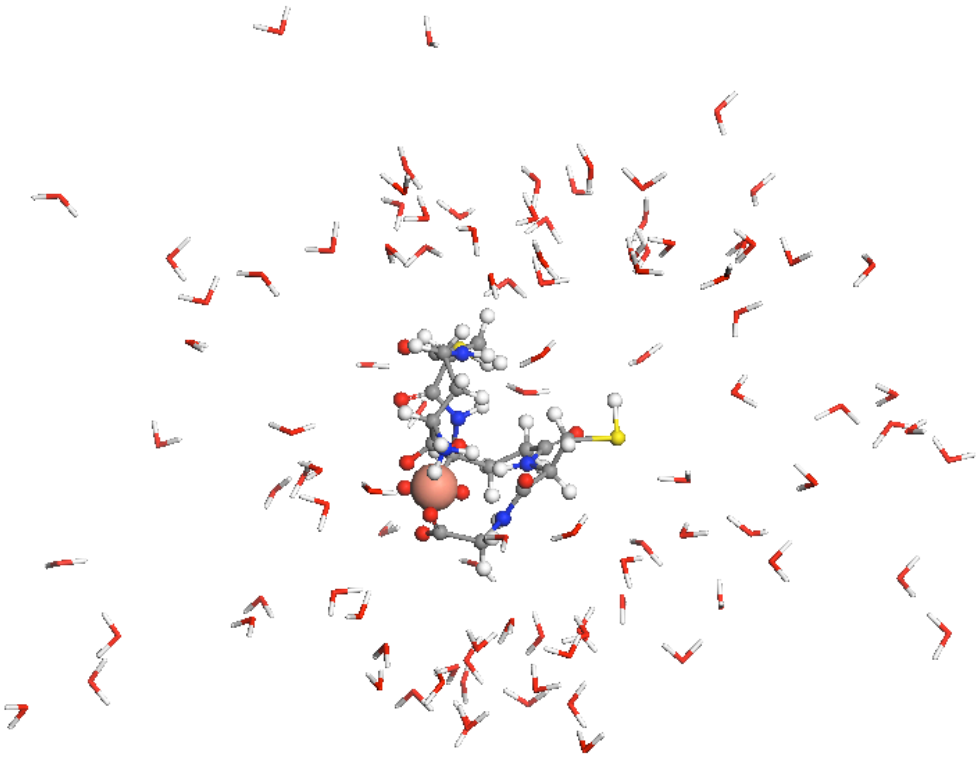

Figure S5. Fully hydrated Cu(II)–PC-2 complex after last MD run. Atom color legend: gray (C), red (O), white (H), yellow (S), brown (Cu^{2+}).

APPENDIX B

STRUCTURES OF METAL–MC-LR COMPLEXES

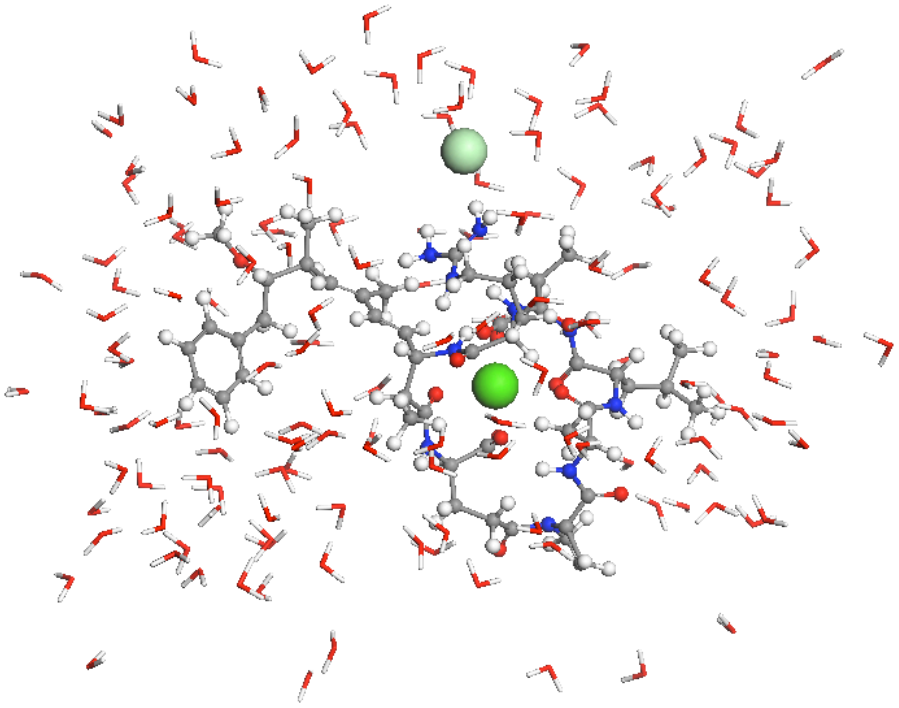

Figure S6. Fully hydrated [Ca–MC-LR]Cl complex after last MD run. Atom color legend: gray (C), red (O), white (H), light green (Cl^-), green (Ca^{2+}).

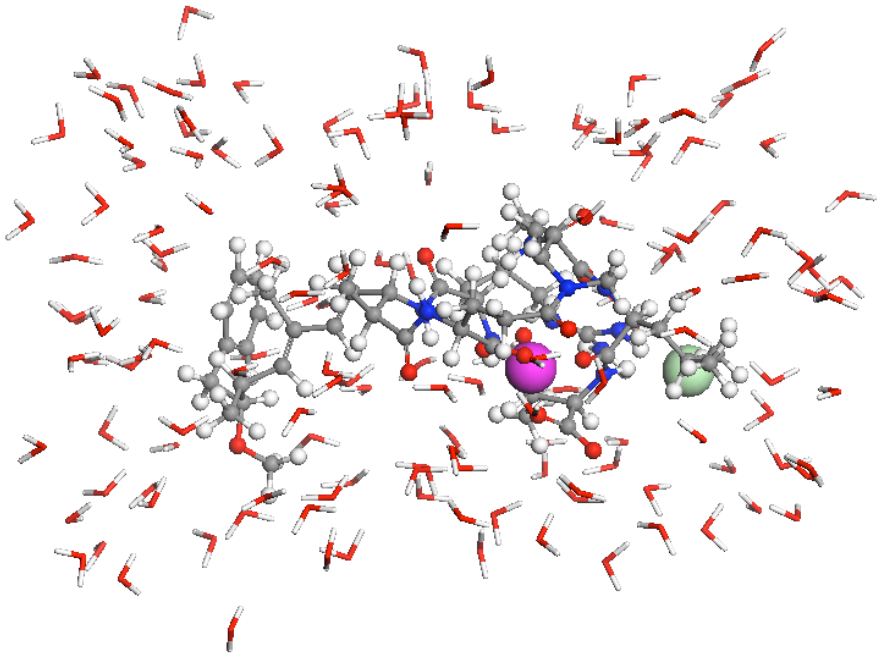

Figure S7. Fully hydrated [Mg–MC-LR]Cl complex after last MD run. Atom color legend: gray (C), red (O), white (H), light green (Cl^-), pink (Mg^{2+}).

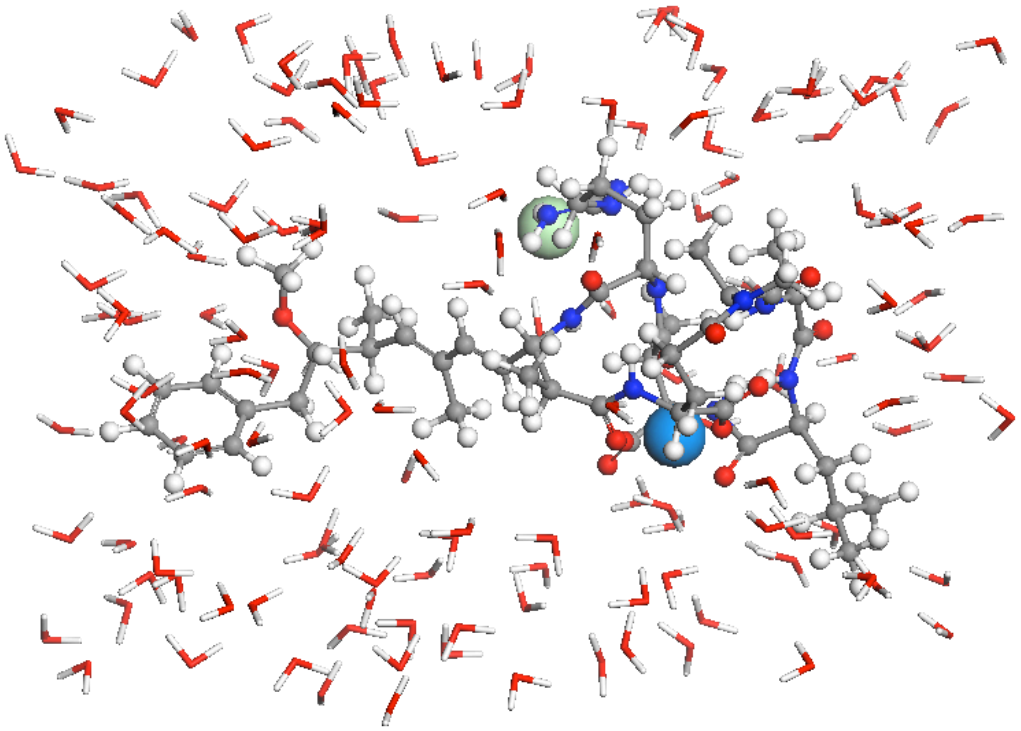

Figure S8. Fully hydrated [Fe(II)–MC-LR]Cl complex after last MD run. Atom color legend: gray (C), red (O), white (H), light green (Cl^-), blue (Fe^{2+}).

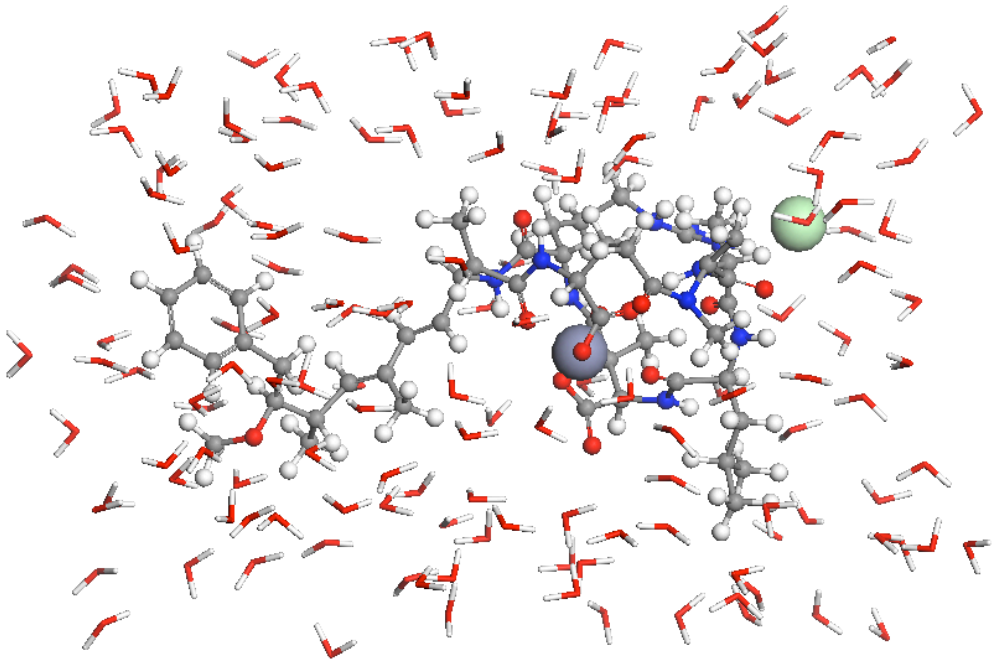

Figure S9. Fully hydrated [Zn(II)–MC-LR]Cl complex after last MD run. Atom color legend: gray (C), red (O), white (H), light green (Cl^-), gray (Zn^{2+}).

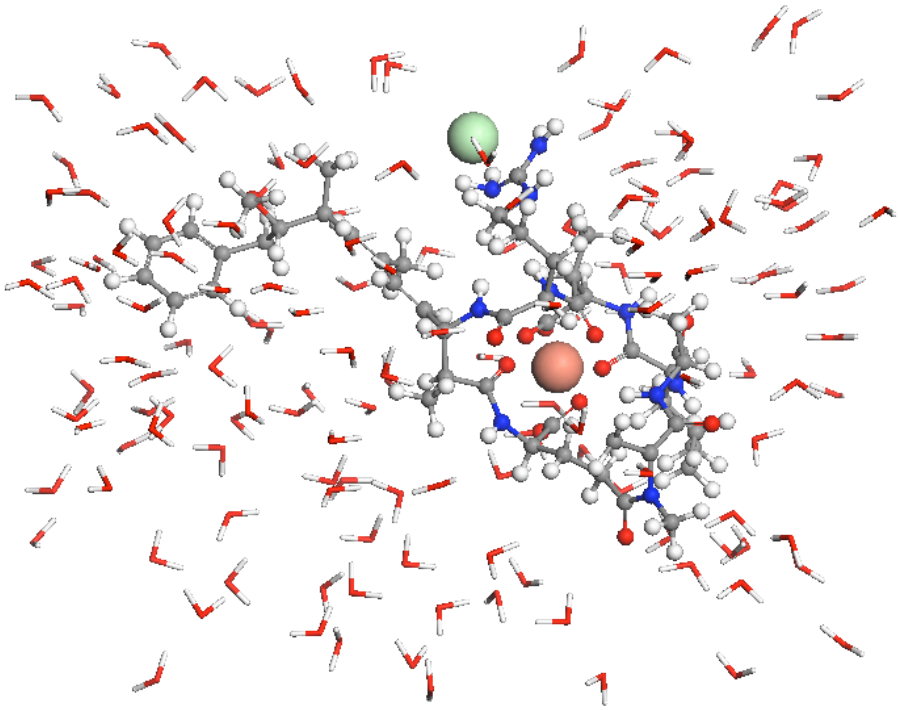

Figure S10. Fully hydrated [Cu(II)–MC-LR]Cl complex after last MD run. Atom color legend: gray (C), red (O), white (H), light green (Cl^{-}), brown (Cu^{2+}).

APPENDIX C

STRUCTURES OF METAL–MC-RR COMPLEXES

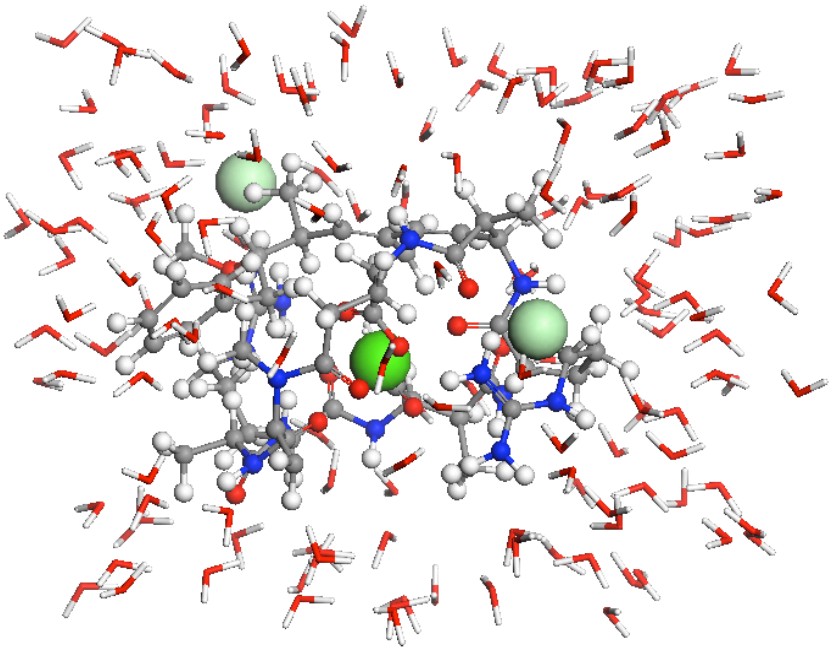

Figure S11. Fully hydrated [Ca–MC-RR]Cl_2 complex after last MD run. Atom color legend: gray (C), red (O), white (H), light green (Cl^-), green (Ca^{2+}).

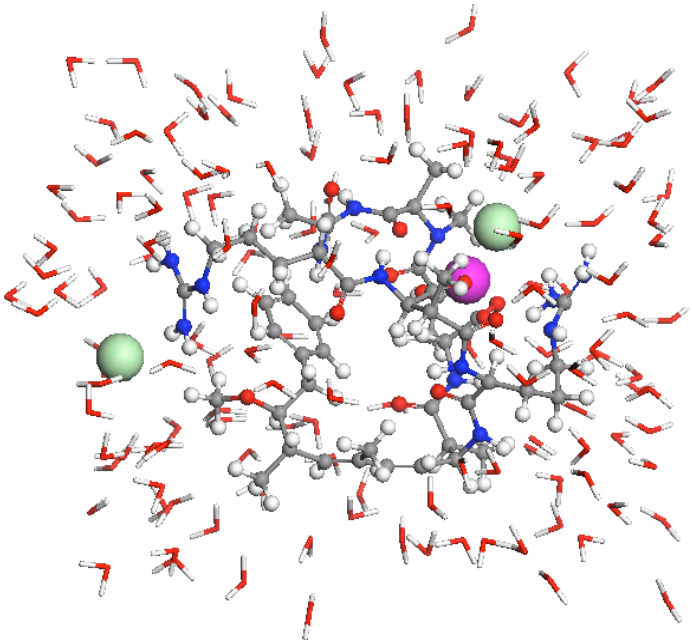

Figure S12. Fully hydrated [Mg–MC-RR]Cl_2 complex after last MD run. Atom color legend: gray (C), red (O), white (H), light green (Cl^-), pink (Mg^{2+}).

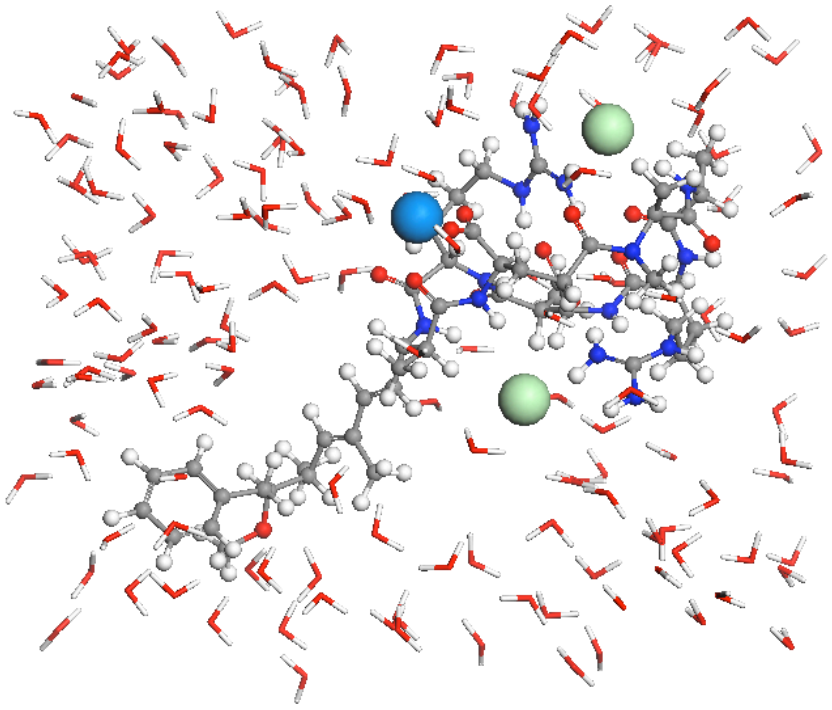

Figure S13. Fully hydrated [Fe(II)–MC-RR]Cl_2 complex after last MD run. Atom color legend: gray (C), red (O), white (H), light green (Cl^-), blue (Fe^{2+}).

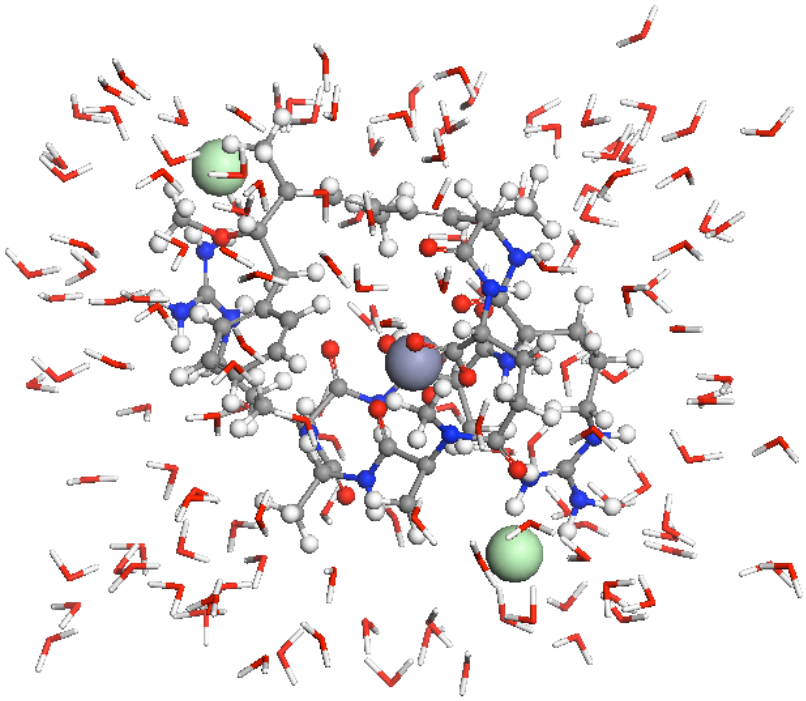

Figure S14. Fully hydrated [Zn(II)–MC-RR]Cl_2 complex after last MD run. Atom color legend: gray (C), red (O), white (H), light green (Cl^-), gray (Zn^{2+}).

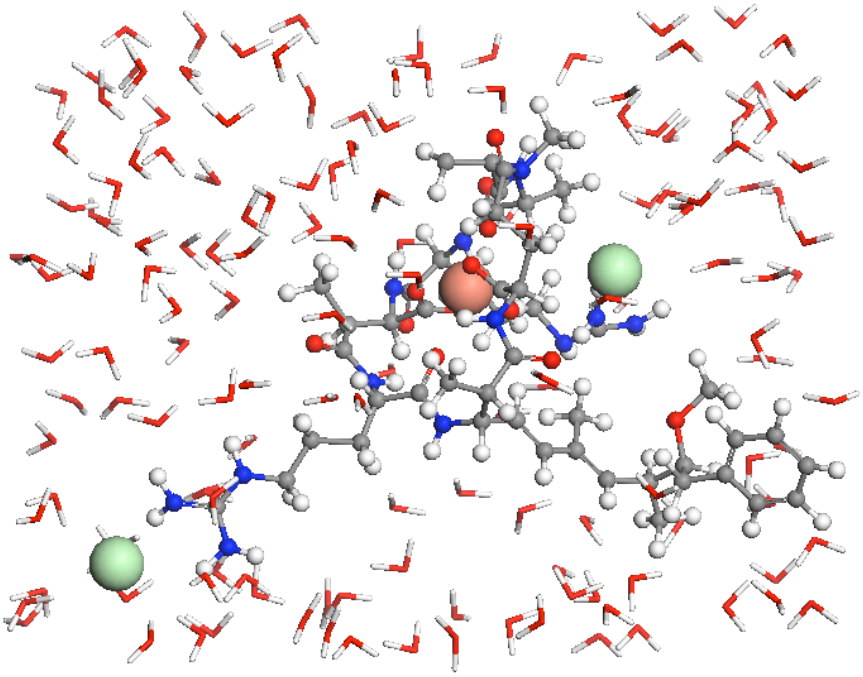

Figure S15. Fully hydrated [Cu(II)–MC-RR]Cl_2 complex after last MD run. Atom color legend: gray (C), red (O), white (H), light green (Cl^-), brown (Cu^{2+}).

REFERENCES

(1) Cowan, J. A. Metal Activation of Enzymes in Nucleic Acid Biochemistry. *Chem. Rev.* **1998**, *98*, 1067–1088.
(2) Shaul, O. Magnesium transport and function in plants: the tip of the iceberg. *Biometals* **2002**, *15*, 309–323.
(3) Droppa, M.; Horváth, G. The role of copper in photosynthesis. *Crit. Rev. Plant. Sci.* **1990**, *9*, 111–123.
(4) Merchant, S.; Bogorad, L. Regulation by copper of the expression of plastocyanin and cytochrome c552 in Chlamydomonas reinhardi. *Mol. Cell. Biol.* **1986**, *6*, 462–469.
(5) Nagajyoti, P. C.; Lee, K. D.; Sreekanth, T. V. M. Heavy metals, occurrence and toxicity for plants: a review. *Environ. Chem. Lett.* **2010**, *8*, 199–216.
(6) Cakmak, I. Tansley Review No. 111. Possible roles of zinc in protecting plant cells from damage by reactive oxygen species. *New Phytol.* **2000**, *146*, 185–205.
(7) Vallee, B. L.; Auld, D. S. Zinc coordination, function, and structure of zinc enzymes and other proteins. *Biochemistry* **1990**, *29*, 5647–5659.
(8) Peterson, H. G.; Healey, F. P. Metal toxicity to algae: a highly pH dependent phenomenon. *Can. J. Fish. Aquat. Sci.* **1984**, *41*, 974–979.
(9) Rauser, W. E. Structure and function of metal chelators produced by plants. *Cell. Biochem. Biophys.* **1999**, *31*, 19–48.
(10) Wei, L. P.; Ahner, B. A. Sources and sinks of dissolved phytochelatin in natural seawater. *Limnol. Oceanogr.* **2005**, *50*, 13–22.
(11) Strasdeit, H.; Duhme, A.-K.; Kneer, R.; Zenk, M. H.; Hermes, C.; Nolting, H.-F. Evidence for discrete Cd(SCys) 4 units in cadmium phytochelatin complexes from EXAFS spectroscopy. *J. Chem. Soc. Chem. Comm.* **1991**, *0*, 1129–1130.
(12) Rauser, W. E. Phytochelatins and related peptides. Structure, biosynthesis, and function. *Plant. Physiol.* **1995**, *109*, 1141–1149.
(13) Dorčák, V.; Krężel, A. Correlation of acid–base chemistry of phytochelatin PC2 with its coordination properties towards the toxic metal ion Cd(II). *Dalton Trans.* **2003**, 2253–2259.
(14) Ginn, H. P.; Pearson, L. A.; Neilan, B. A. Hepatotoxin biosynthesis and regulation in cyanobacteria–the putative involvement of nitrogen and iron homeostasis mechanisms. *Chiang Mai J. Sci.* **2009**, *36*, 200–223.
(15) Pflugmacher, S. Possible allelopathic effects of cyanotoxins, with reference to microcystin-LR, in aquatic ecosystems. *Environ. Toxicol.* **2002**, *17*, 407–413.
(16) Humble, A. V.; Gadd, G. M.; Codd, G. A. Binding of copper and zinc to three cyanobacterial microcystins quantified by differential pulse polarography. *Water Res.* **1997**, *31*, 1679–1686.
(17) Saito, K.; Sei, Y.; Miki, S.; Yamaguchi, K. Detection of microcystin–metal complexes by using cryospray ionization-Fourier transform ion cyclotron resonance mass spectrometry. *Toxicon* **2008**, *51*, 1496–1498.
(18) Klein, A. R.; Baldwin, D. S.; Silvester, E. Proton and iron binding by the cyanobacterial toxin microcystin-LR. *Environ. Sci. Technol.* **2013**, *47*, 5178–5184.
(19) Pearson, L. A.; Hisbergues, M.; Börner, T.; Dittmann, E.; Neilan, B. A. Inactivation of an ABC transporter gene, mcyH, results in loss of microcystin production in the cyanobacterium Microcystis aeruginosa PCC 7806. *Appl. Environ. Microbiol.* **2004**, *70*, 6370–6378.
(20) Daly, R. I.; Ho, L.; Brookes, J. D. Effect of chlorination on Microcystis aeruginosa cell integrity and subsequent microcystin release and degradation. *Environ. Sci. Technol.* **2007**, *41*, 4447–4453.

(21) Young, F. M.; Thomson, C.; Metcalf, J. S.; Lucocq, J. M.; Codd, G. A. Immunogold localisation of microcystins in cryosectioned cells of Microcystis. *J. Struct. Biol.* **2005**, *151*, 208–214.
(22) Pickering, I. J.; Prince, R. C.; George, G. N.; Rauser, W. E.; Wickramasinghe, W. A.; Watson, A. A.; Dameron, C. T.; Dance, I. G.; Fairlie, D. P.; Salt, D. E. X-ray absorption spectroscopy of cadmium phytochelatin and model systems. *BBA–Protein Struct. M.* **1999**, *1429*, 351–364.
(23) Yan, F.; Ozsoz, M.; Sadik, O. A. Electrochemical and conformational studies of microcystin-LR. *Anal. Chim. Acta* **2000**, *409*, 247–255.
(24) Song, W.-Y.; Park, J.; Mendoza-Cozatl, D. G.; Suter-Grotemeyer, M.; Shim, D.; Hoertensteiner, S.; Geisler, M.; Weder, B.; Rea, P. A.; Rentsch, D.; et al. Arsenic tolerance in Arabidopsis is mediated by two ABCC-type phytochelatin transporters. *Proc. Natl. Acad. Sci. U.S.A.* **2010**, *107*, 21187–21192.
(25) Vatamaniuk, O. K.; Bucher, E. A.; Sundaram, M. V.; Rea, P. A. CeHMT-1, a putative phytochelatin transporter, is required for cadmium tolerance in Caenorhabditis elegans. *J. Biol. Chem.* **2005**, *280*, 23684–23690.
(26) Munusamy, T.; Hu, Y.-L.; Lee, J.-F. Adsorption and photodegradation of microcystin-LR onto sediments collected from reservoirs and rivers in Taiwan: a laboratory study to investigate the fate, transfer, and degradation of microcystin-LR. *Environ. Sci. Pollut. Res. Int.* **2012**, *19*, 2390–2399.
(27) Wu, X.; Xiao, B.; Li, R.; Wang, C.; Huang, J.; Wang, Z. Mechanisms and Factors Affecting Sorption of Microcystins onto Natural Sediments. *Environ. Sci. Technol.* **2011**, *45*, 2641–2647.
(28) Chen, W.; Song, L.; Peng, L.; Wan, N.; Zhang, X.; Gan, N. Reduction in microcystin concentrations in large and shallow lakes: Water and sediment-interface contributions. *Water Res.* **2008**, *42*, 763–773.
(29) Sun, H. COMPASS: An ab initio force-field optimized for condensed-phase applications overview with details on alkane and benzene compounds. *J. Phys. Chem. B* **1998**, *102*, 7338–7364.
(30) Accelrys Software Inc., Materials Studio Modeling Environment, Release 7.0, San Diego: Accelrys Software Inc., 2013.
(31) Yang, J.; Ren, Y.; Tian, A.; Sun, H. COMPASS force field for 14 inorganic molecules, He, Ne, Ar, Kr, Xe, H2, O2, N2, NO, CO, CO2, NO2, CS2, and SO2, in liquid phases. *J. Phys. Chem. B* **2000**, *104*, 4951–4957.
(32) McQuaid, M. J.; Sun, H.; Rigby, D. Development and validation of COMPASS force field parameters for molecules with aliphatic azide chains. *J. Comput. Chem.* **2004**, *25*, 61–71.
(33) Aristilde, L.; Sposito, G. Molecular modeling of metal complexation by a fluoroquinolone antibiotic. *Environ. Toxicol. Chem.* **2008**, *27*, 2304–2310.
(34) Grill, E.; Löffler, S.; Winnacker, E. L.; Zenk, M. H. Phytochelatins, the heavy-metal-binding peptides of plants, are synthesized from glutathione by a specific gamma-glutamylcysteine dipeptidyl transpeptidase (phytochelatin synthase). *Proc. Natl. Acad. Sci. U.S.A.* **1989**, *86*, 6838–6842.
(35) Kassaar, O.; McMahon, S. A.; Thompson, R.; Botting, C. H.; Naismith, J. H.; Stewart, A. J. Crystal structure of histidine-rich glycoprotein N2 domain reveals redox activity at an interdomain disulfide bridge: implications for angiogenic regulation. *Blood* **2014**, *123*, 1948–1955.
(36) Bagu, J. R.; Sönnichsen, F. D.; Williams, D.; Andersen, R. J.; Sykes, B. D.; Holmes, C. F. B. Comparison of the solution structures of microcystin-LR and motuporin. *Nat. Struct. Biol.* **1995**, *2*, 114–116.

(37) Vinogradov, E. V.; Smirnov, P. R.; Trostin, V. N. Structure of hydrated complexes formed by metal ions of Groups I—III of the Periodic Table in aqueous electrolyte solutions under ambient conditions. *Russ. Chem. B.* **2003**, *52*, 1253–1271.
(38) Ohtaki, H.; Radnai, T. Structure and dynamics of hydrated ions. *Chem. Rev.* **1993**, *93*, 1157–1204.
(39) Enami, I.; Akutsu, H.; Kyogoku, Y. Intracellular pH Regulation in an Acidophilic Unicellular Alga, Cyanidium caldarium: 31P-NMR Determination of Intracellular pH. *Plant Cell. Physiol.* **1986**, *27*, 1351–1359.
(40) Giraldez-Ruiz, N.; Mateo, P.; Bonilla, I.; Fernandez-Piñas, F. The relationship between intracellular pH, growth characteristics and calcium in the cyanobacterium Anabaena sp. strain PCC7120 exposed to low pH. *New Phytol.* **1997**, *137*, 599–605.
(41) Kurkdjian, A.; Guern, J. Intracellular pH: Measurement and Importance in Cell Activity. *Annu. Rev. Plant. Physiol. Plant. Mol. Biol.* **1989**, *40*, 271–303.
(42) Spain, S. M.; Rabenstein, D.L. Characterization of the Acid/Base and Redox Chemistry of Phytochelatin. *Anal. Chem.* **2003**, *75*, 3712–3719.
(43) Haas, D. J.; Harris, D. R.; Mills, H. H. The crystal structure of guanidinium chloride. *Acta crystallogr.* **1965**, *19*, 676–679.
(44) Sutton, R.; Sposito, G.; Diallo, M. S.; Schulten, H. R. Molecular simulation of a model of dissolved organic matter. *Environ. Toxicol. Chem.* **2005**, *24*, 1902–1911.
(45) Accelrys Software Inc., Discovery Studio Modeling Enrivonment, Release 4.0, San Diego: Accelrys Software Inc., 2013.
(46) Shtyrlin, V. G.; Zyavkina, Y. I.; Ilakin, V. S.; Garipov, R. R. Structure, stability, and ligand exchange of copper (II) complexes with oxidized glutathione. *J. Inorg. Biochem.* **2005**, *99*, 1335–1346.
(47) Li, N. C.; Manning, R. A. Some Metal Complexes of Sulfur-containing Amino Acids1, 2. *J. Am. Chem. Soc.* **1955**, *77*, 5225.
(48) Harris, D. C. *Exploring Chemical Analysis*; 4th ed.; W. H. Freeman and Company, 2009.
(49) Kirkby, E. A.; Pilbeam, D. J. Calcium as a plant nutrient. *Plant Cell Environ.* **1984**, *7*, 397–405.
(50) Bourg, I. C.; Sposito, G. Molecular dynamics simulations of the electrical double layer on smectite surfaces contacting concentrated mixed electrolyte (NaCl-CaCl2) solutions. *J Colloid Interf. Sci.* **2011**, *360*, 701–715.
(51) Calvo, R.; Steren, C. A.; Piro, O. E.; Rojo, T.; Zuniga, F. J.; Castellano, E. E. Crystal structure and magnetic properties of diaqua(L-aspartato)copper(II). *Inorg. Chem.* **2002**, *32*, 6016–6022.
(52) Harding, M. M. Geometry of metal–ligand interactions in proteins. *Acta Crystallogr. D* **2001**, *57*, 401–411.
(53) Aristilde, L.; Sposito, G. Binding of ciprofloxacin by humic substances: A molecular dynamics study. *Environ. Toxicol. Chem.* **2010**, *29*, 90–98.
(54) Duckworth, O. W.; Bargar, J. R.; Sposito, G. Quantitative-Structure Activity Relationships for Aqueous Metal-Siderophore Complexes. *Environ. Sci. Technol.* **2009**, *43*, 343–349.
(55) Dainty, J. Ion transport and electrical potentials in plant cells. *Annu. Rev. Plant Phys.* **1962**, *13*, 379–402.
(56) Sposito, G. *The Chemistry of Soils*, 2nd ed.; Oxford University Press: USA, 2008.